공학석사 학위논문

TiO_2 Nanoparticles Attached on a Superparamagnetic Iron Oxide Nanocluster Core@Fibrous Silica Shell Nanocomposite as a Magnetically Recoverable Photocatalyst

초상자성 산화철 나노클러스터 중심@방사형
실리카 피막의 나노복합체에 이산화티타늄
나노입자가 부착된 재사용이 가능한 광촉매에
대한연구

2017년 2월

서울대학교 대학원

융합과학부 나노융합전공

서 보 경

Abstract

TiO_2 Nanoparticles Attached on a Superparamagnetic Iron Oxide Nanocluster Core@Fibrous Silica Shell Nanocomposite as a Magnetically Recoverable Photocatalyst

Bokyung Seo

Program in Nano Science and Technology

Department of Transdisciplinary Studies

The Graduate School of Convergence Science and Technology

Seoul National University

A magnetically recoverable photocatalyst was prepared by supporting TiO_2 nanoparticles on a superparamagnetic iron oxide nanocluster (SION) core@fibrous silica shell (FSS) nanocomposite. Using the raspberry-shaped magnetic iron oxide nanocluster core as a seed, FSS with uniform thickness was grown directly on the core surface by a sol-gel process. The preparation method was optimized to have a single core for each nanoparticle by adjusting the amount of the silica source. The FSS has a fanning structure of radial pores, which enable large amounts of TiO_2 nanoparticles to be supported easily on the pore surface. SION@FSS with amorphous TiO_2 loaded on the pores (SION@FSS@Am-TiO_2) was crystallized to the anatase phase (SION@FSS@A-TiO_2), which shows good photocatalytic effect.

When used for water purification, SION@FSS@A-TiO_2 shows faster dye degradation kinetics compared to commercial P25 nanoparticles. The as-prepared SION@FSS@A-TiO_2 photocatalyst could be magnetically recovered easily from water after decolorization of dye.

Keywords: Fibrous silica nanoparticle, Photocatalyst, Core shell, Dye degradation, Reusable nanoparticle

Student Number : 2014-24838

Contents

List of Tables

List of Figures

Chapter 1. Introduction

1.1. TiO_2 Photocatalyst

As per World Bank estimates, up to 30 percent of water pollution among G20 country is contributed by wastewater from textile industry [1,2]. Textile effluents may cause bladder cancer to workers in dyeing and printing section [3] and it can even harm ocean animals [4]. Therefore, a number of studies have focused on purifying textile effluents. There are many techniques for decolorization of dye from wastewater, and these include physical, electrochemical/chemical, biological and photocatalytic methods. Usually, a combination of processes is necessary because using a single method alone has its constraints. One of the combined techniques is the use of UV-illuminated titania (UV/TiO_2) as a photocatalyst after aerobic biological oxidation [5]. In a bio-photoreactor system, UV/TiO_2 can degrade nonbiodegradable molecules after a biological process [6]. Anatase phase TiO_2 is widely used because it has high photocatalytic activity than that of rutile [7] and its low cost.

1.2. Mesoporous silica (MSN) supports

The growing use of TiO_2 as a catalyst has given rise to increasing concerns regarding the inflammatory response [8, 9] and adverse effects [10] of anatase TiO_2. Therefore, TiO_2 nanoparticles that remain in water after the purification step can pose problems, especially those in the ultrafine size regime (25 nm) [11]. From this point of view, there has been a continued effort to recollect TiO_2 nanoparticles by immobilizing them on solid supports [12, 13]. When using mesoporous silica nanoparticles (MSNs) (**Figure 1**) [14, 15] as a solid support [16, 17], TiO_2 clusters can be confined into the nanopores, preventing aggregation and enhancing the catalytic effect [18]. As a host

material, the direction, shape [19], and size [20] of the MSN pore determines the size and amount of confined TiO_2.

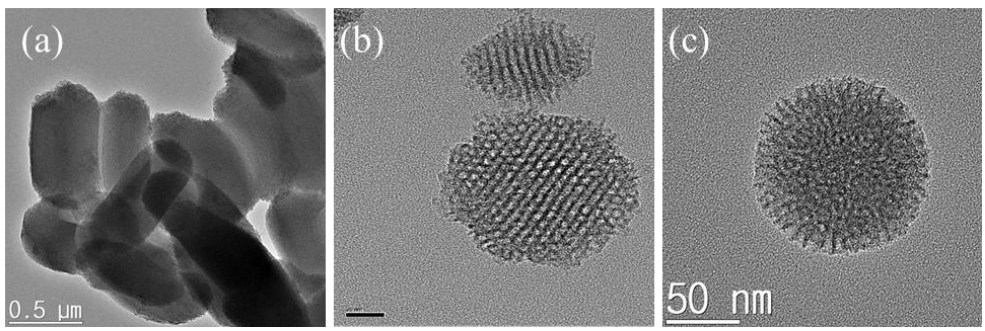

Figure 1 Various mesoporous silica nanoparticles (a) SBA-15 (cylindrical pore), (b) MCM-41 (cylindrical pore) and (c) fibrous shaped nanoparticle with radial pore.

1.3. Fibrous silica materials

1.3.1. Characteristics and applications

Fibrous silica materials (**Figure 1** (a)) [21], also called as dendritic silica nanomaterials [22] or hierarchical mesoporous silica nanoparticles [23,24], have a fanning structure of radial pores that are aligned perpendicularly [25]. Easily accessible pores enabled its enhanced adsorption and release ability than that of counterparts [22]. As a support for TiO_2 photocatalyst, it increases the loading of TiO_2 and enhance the catalytic effect than that of conventional MSNs [19]. The fibrous structure also makes them suitable for kinds of applications including catalyst [26], column in liquid chromatography [27] and excellent superhydrophilic material [28].

1.3.2. Synthesis

During the synthesis of fibrous silica nanomaterials, an oil-water dual solvent is used with a catalyst, surfactant, and tetraethyl orthosilicate (TEOS) as a silica precursor. Polshettiwar et al. [21] prepared silica spheres with radially oriented channels using a microwave-assisted hydrothermal technique. In that study, the sphere has an overall size of 250-450 nm and dendritic fibers of 8-10 nm thickness. The authors observed a highly fibrous structure on increasing the urea to TEOS ratio. Mesoporous to wrinkled fibrous nanoparticles were obtained [23] by increasing the oil to water ratio. By changing the oil-water-surfactant ratio, the authors found that a fibrous morphology could be obtained in a bicontinuous micro emulsion phase. Small-sized fibrous silica spheres (130 nm) were synthesized [29] using cetyltrimethyl-ammonium tosylate as a surfactant. When cetyltrimethylammonium bromide (CTAB) was used as a surfactant, the surface areas and pore size were increased as the concentration of small organic amines increased. Raspberry and worm-like structures were obtained when using CTAB with triethyleneamine (TEA) or triethanolamine (TEAH) respectively. The larger surface area and pore volume obtained for the raspberry or worm-like structures were owing to the thinner and connected walls in these structures. In another work, the dependence of the connectivity of fibrous silica spheres on the phase behavior of the oil-water-surfactant system has been studied [30]. The results show that the oil-water-surfactant ratio is an important factor determining the pore size and pore volume of fibrous silica nanoparticles synthesized in a bicontinuous (Windsor II) system. By changing the oil-solvent composition, multigenerational fibrous silica spheres were synthesized that enabled pore size tuning from 2.8 to 13 nm [31]. For each generation, the thickness of the layer was controlled from 5 to 180 nm depending on the reaction

time and the amount of the silica source. Therefore, these spheres showed a high bovine β-lactoglobulin loading capacity.

1.4. **Magnetically recoverable photocatalyst**

1.4.1. Magnetic recollection

Still, the key issue remains when separating TiO_2 with MSN support from purified water. Since this separation requires filtering or centrifugation, separating catalyst nanoparticles from a large quantity of solution is not very suitable. As an alternative, magnetic nanoparticles were embedded in the catalysts for magnetic recollection [32, 33, 34, 35, 36, 37, 38, 39]. When the size of magnetic nanoparticles is in between 10–20 nm and remains constant above the blocking temperature, the nanoparticles have a single magnetic domain and show superparamagnetism [40]. Superparamagnetic nanoparticles have large magnetic moment without coercivity and have remnant magnetism close to zero [40]. Hence, such superparamagnetic nanoparticles can be used in biomedical and environmental applications. When a magnetic field is applied, superparamagnetic nanoparticles face a high magnetic moment, which is advantageous for magnetic separation/recollection. In contrast, when the magnetic field is removed, magnetic nanoparticles lose their magnetism and hence their aggregation reduces [40].

1.4.2. Superparamagnetic iron oxide nanocluster (SION) core

Superparamagnetic iron oxide nanoclusters (SIONs) which consists of small magnetic grains recently attracted much research interest [41, 42]. Contrary to the ferromagnetic behavior of iron oxide with the same size, magnetic interaction among

grains within the nanocluster results in a superparamagnetic behavior of the nanocluster [41]. These nanoclusters combine the advantages of individual grains and result in an enhanced magnetic property [42].

1.4.3. SION Core@Fibrous Silica Shell (FSS)

Nanoparticle separation performed with SIONs core coated with easily accessible FSS is suitable for catalyst recollection where significant mass transport is essential. About coating FSS on dense amorphous silica pre-coated magnetic nanoparticles, there are several reports [43,44,45]. Direct synthesis of FSS on an iron oxide nanocore is also investigated [46].

When a silica shell was coated on magnetic nanoparticle [47,48,49,50], magnetic properties can be engineered. Saturation magnetization could enhance after annealing SION coated with the silica shell because of reduced particle–particle interactions [47]. In that work, a decrease in the blocking temperature of the annealed sample was observed. Similarly, increased magnetization and increased surface spins was reported after sol-gel combustion synthesis of hematite nanoparticles embedded in silica nanostructures [49]. When controlling the thickness of silica shell on a SION cluster, saturation magnetization decreased with the increasing shell area compared to the SION core area [48]. Those articles show that it is possible to change the magnetic property of magnetic core@ silica shell nanoparticles. By magnetic property engineering, the SION core coated with a silica shell can be designed to fit suitable applications such as biomedical applications, bio-separation, and nanoparticle recollection. In this regard, photocatalyst-supported magnetic core@ silica shell nanoparticles can be designed to fit the bio-photoreactor system [6]. Using an additional magnetic separation device, both bio-degradable and non-

biodegradable molecules in wastewater can be purified, without producing any photocatalyst nanoparticle/nanocomposite sludge.

1.4.4. SION@FSS@Anatase TiO_2 (A-TiO_2)

In this work, we applied a biphase stratification approach [31] to grow a FSS on the SION core up to the third generation. The results show that a FSS layer with easily accessible high surface areas was successfully generated on the SION. TiO_2 nanoparticles were further loaded on the radial pore surface to generate a magnetically recoverable photocatalyst (SION@FSS@A-TiO_2). The SION@FSS@A-TiO_2 photocatalyst shows higher dye degradation kinetics than that of commercial P25 nanoparticles when used for water purification.

Chapter 2. Experimental

2.1. Materials

Ethylene glycol (99.9%), ethyl alcohol (ETOH) (95.0%), acetone (99.5%), cyclohexane (99.0%) and hydrochloric acid (35-37 %) were obtained from Samchun. Iron (Ⅲ) chloride hexahydrate (97.0%), sodium citrate tribasic dehydrate (≥99.0%), triethanolamine (TEA, 98%), sodium acetate (99%), 1-octadecene (90%), hydroxyl propyl cellulose (HPC), titanium butoxide (TBOT, 97%), titanium (IV) oxide (Aeroxide® P25), and methylene blue solution (MetB, 1.5g/100mL) were purchased from Sigma Aldrich. CTAB and TEOS (98%) were obtained from Across. Decahydronaphthalene (97%) was obtained from Junsei. All reagents were used without further purification unless specified.

2.2. Preparation of SION

The iron oxide nanocluster cores were synthesized by following a previously reported procedure [51]. Briefly, 1.95 g of iron (Ⅲ) chloride hexahydrate, 0.6 g of sodium citrate tribasic dehydrate, and 60 ml of ethylene glycol were mixed with magnetic stirrer. When 3.6 g of sodium acetate was added to the solution, the color of the mixture was changed from yellowish red to yellowish brown. After stirring for 30 min, the resulting mixture was poured into a 100 ml stainless steel autoclave equipped with a Teflon liner. Next, the Teflon lined autoclave was heated in a 200 °C oven. After 10 h of the hydrothermal reaction, the black precipitate was dispersed in distilled water. After washing for 3 times with water and acetone, the resulting SION was dispersed in distilled water with the concentration of 9.3 mg/mL.

2.3. **Preparation of SION@FSS**

The FSS was generated on the SION by following a previously reported procedure [31]. Typically, 200 ml of the SION colloid, 416 ml of distilled water, 92.9 g of CTAB and 2.5 g of TEA were mixed in a 2 L multi-neck reaction flask. The mixture was heated to 60 °C for 30 min and maintained at that temperature with overhead stirrer (OS40-Pro, Proneer, Korea) accompanied with PTFE impeller of 8 mm shaft length. After an hour, 685 μl of TEOS in 274 ml of 1-octadecene was added to the solution. After stirring for 12 h, the oil phase layer was discarded and replaced with 685 μl of TEOS in 274 ml of decahydronaphthalene. The mixture was reacted for another 12 h at 60 °C to generate a fibrous silica coating layer again. Then, the oil phase layer was removed again and 685 μl of TEOS in 274 ml of cyclohexane was added to the mixture solution to further grow the silica layer. The final reaction was carried out at 60 °C for another 12 h. At the end of the reaction, an excess amount of ethanol was added to the mixture solution. After centrifugation (10000 RPM, 30 min), the pellet was redispersed in ethanol, washed with ethanol and distilled water two times, and then dried in a 60 °C oven. To remove residual CTAB, the resulting brown powder was collected and calcinated in a tube furnace at 550 °C for 5 h. The final product was named as SION@FSS.

2.4. Preparation of SION@FSS@Am-TiO_2 and SION@FSS@A-TiO_2

110 mg of SION@FSS, 0.6 mg of HPC, and 100 µL of distilled water were dispersed in 200 ml of ethanol. The mixture was mixed vigorously using an overhead stirrer for the entire duration of the reaction. The solution was heated to 85 °C and maintained at that temperature for 1 h. After mixing 800 µl of TBOT with 10 ml ethanol, the solution was added dropwise using a syringe pump at a flow rate of 0.5 ml/min. The mixture was followed by refluxing at 85 °C for 100 min. After the reaction, the resulting nanoparticles were washed first with methanol and then with ethanol twice. The products were sonicated for 10 min to enhance the surface area of the TiO_2 nanoparticles [52] followed by centrifugation (10000 RPM, 30 min). The pellet (SION@FSS@Am-TiO_2) was collected and redispersed in ethanol. After a hydrothermal reaction at 180 °C for 1.5 h, the final nanoparticle composites were denoted as SION@FSS@A-TiO_2. Synthesis conditions from SION to SION@FSS@A-TiO2 synthesis is summarized in Table 1.

Table 1 Summary of synthesis conditions

Synthesis Step	Sample Name	Nanoparticle	TEOS [µl]	CTAB [g]	TEA [g]	TBOT [µl]	HPC [mg]	Temp. (˚C)	Reaction Time	Water	Solvent
1	SION§§	-	-	-	-	-	-	200	10 hour	-	-
2-1 (1st FSS Generation)						-	-				274 ml 1-Octadecene§
2-2 (3rd FSS Generation)	SION@FSS¶	200 ml SION† (9.3mg/ml)	685†	92.9*	2.5*	-	-	60	12 hour	416 ml	274 ml Decalin§
2-3 (3rd FSS Generation)						-	-				274 ml Cyclohexane§
3 (CTAB removal)	SION@FSS (powder)¶¶	SION@FSS (dried in 60 ˚C oven)	-	-	-	-	-	550	5 hour	-	-
4	SION@FSS @Am-TiO_2††	110 mg SION @FSS	-	-	-	800	0.6	85	100 min	100 µl	200 ml Ethanol 100 µl DI Water
5	SION@FSS@A-TiO_2§§	SION@FSS @Am-TiO_2	-	-	-	-	-	180	1.5 hour	-	Ethanol

***** The reagent is added once in the 1st FSS layer generation and the remaining is used in the 2nd and 3rd FSS layer generation.

† The reagent is added in each FSS stratification step.

§ The reagent is added in each FSS stratification step and discarded at the end of each layer generation step

¶ Reaction in a 2L multi-neck flask with mechanical stirring.

†† In a 500 ml round bottom flask with reflux and mechanical stirring.

§§ Hydrothermal reaction

¶¶ Annealed in a tube furnace

2.5. **FSS thickness control of SION@FSS**

For the control of FSS thickness on SION core, the amount of TEOS is controlled while reducing the batch volume. Only the amounts of nanoparticles and batch size (250ml round-bottom-flask) and reagents are changed in the above procedure, Preparation of SION@FSS. In detail, 14.6ml of SION colloid (9.3 g/ml) dispersed in DI water, 30 ml of additional DI water, 6.78 g of CTAB, 0.18 of TEA and 20ml of oil solvents (1-Octadecene and Cyclohexane) are used. FSS control is tested separately initially on a small scale in 500 ml RBF, which is a different procedure from that carried out in the 2 L multi-neck reaction flask.

2.6. **Material Characterization**

The morphology and size of the particles were observed with both a transmission electron microscope (TEM) and field emission scanning electron microscope (FE-SEM). TEM images were taken using JEM-2100F (JEOL). Selected area electron diffraction (SAED) measurements were performed using the same TEM device. A Hitachi/Brucker S-4800/Quantax200 was used to obtain FE-SEM images. Every sample was coated with platinum using a Pt coater (Leica) prior to FE-SEM image acquisition. To make the sample more conductive, the sample was pretreated with 15 mA current for 100 seconds before Pt coating. Energy-dispersive X-ray spectroscopy (EDX) was used for chemical characterization, and elemental analysis was carried out using a Quantax200 (Hitachi). A zeta-potential and particle size analyzer (Otsuka Electronics, Japan) was used to measure the hydrodynamic size of the nanoparticles using dynamic light scattering (DLS). The Brunauer-Emmett-Teller (BET) specific surface area, adsorption isotherm, and pore size distribution at

77.35 K were measured with a BELSORP-max and ASAP 2420. X-ray diffraction (XRD) patterns were obtained using a New D8 Advance diffractometer. During the scan, the incident angle was varied from 20° to 80° at a scanning rate of 2° per min. The magnetic property of the nanoparticle was characterized using a PPMS 14 T (Quantum Design, San Diego), from which we obtained a DC magnetization (M) versus magnetic field graph from 0 T to 14 T.

2.7. **Photodecolorization Test**

The dye degradation test was performed using UV transilluminators as a UV light source. WUV-M20 (WiseUV) is geared with 6 pieces of 8 W UV lamps radiating 312 nm light over an area of 350 mm× 275 mm with 100% intensity (50 mW/cm^2). MetB containing 0.1mg/mL of catalyst nanoparticles in 100 ml ethanol solution was firstly prepared in 100 ml vial. Next, the mixture is stirred in the dark on a multi-axle roller-mixer (RM 5-40, LAT and Raczek analysis GmbH, Germany).

After 2h, the mixture is transferred to 500 ml a 2-neck round bottom flask. Together with UV irradiation, mechanical stirring (200 RPM) and refluxing (**Figure 2**), 1 ml aliquots were withdrawn at designated intervals and centrifuged (10000 RPM, 30 min). The absorbance of the supernatants was measured using a UV-VIS spectrophotometer (UV-1700, Shimadzu).

The Absorbance vs. concentration (mg/L) curve were obtained and linear fitted (**Figure 3**) to obtain the equation for compute unknown concentration from absorbance of a sample. Comparison of reaction rate with Aeroxide® P25 was performed by applying pseudo-first-order kinetics. The rate constant was calculated

from the slope of $\ln(\frac{C}{C_0})$ versus the photocatalytic reaction time. c_0 and c indicate the initial concentration and concentration at time t, respectively.

2.8. **Recollection and Reusability Test**

To test recyclability, the MetB solution containing catalyst nanoparticles was placed under a UV lamp for 30 min. Nanoparticles were separated using a small handheld magnet. Finally, the supernatant was taken and the absorbance spectrum was measured. The nanoparticle pellets were redispersed in the MetB solution to repeat UV illumination. The above procedures were repeated to examine the reusability.

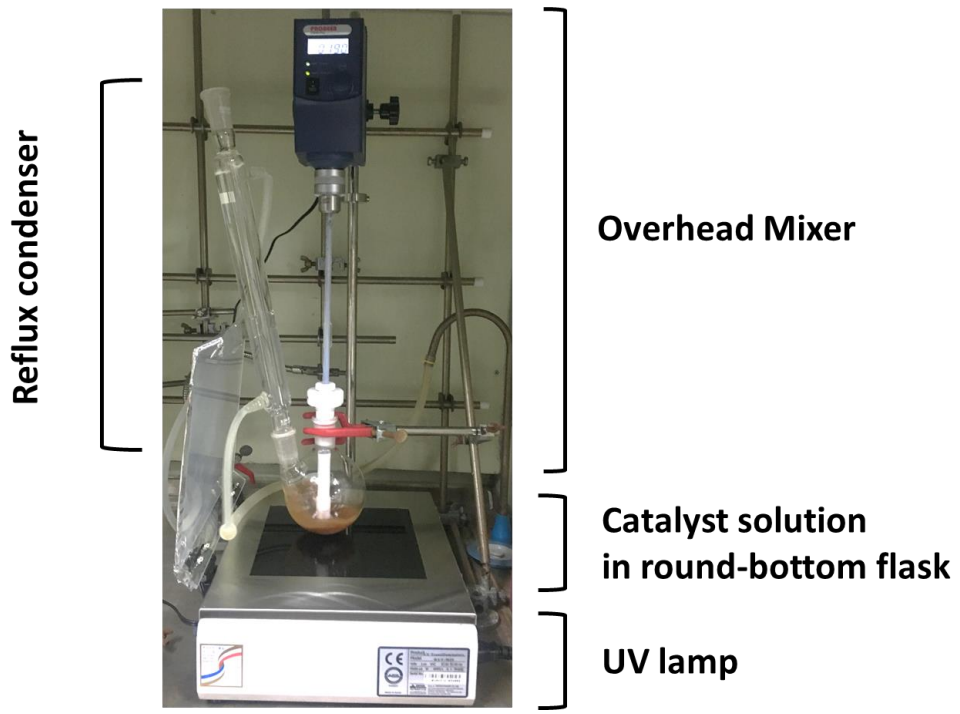

Figure 2 The digital image of photo-reactor system. The system was covered with aluminum foil during UV-illumination to avoid exposure to UV light and shield plastic and rubber components.

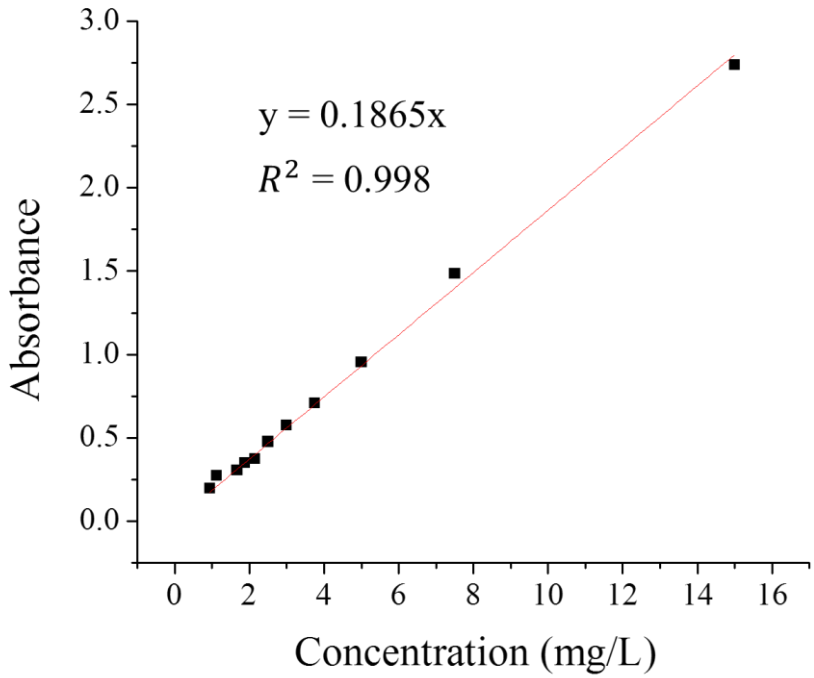

Figure 3 The Calibration curve of methylene blue and the linear fitting result

Chapter 3. Result and discussion

3.1. Synthetic procedures

3.1.1. Overview

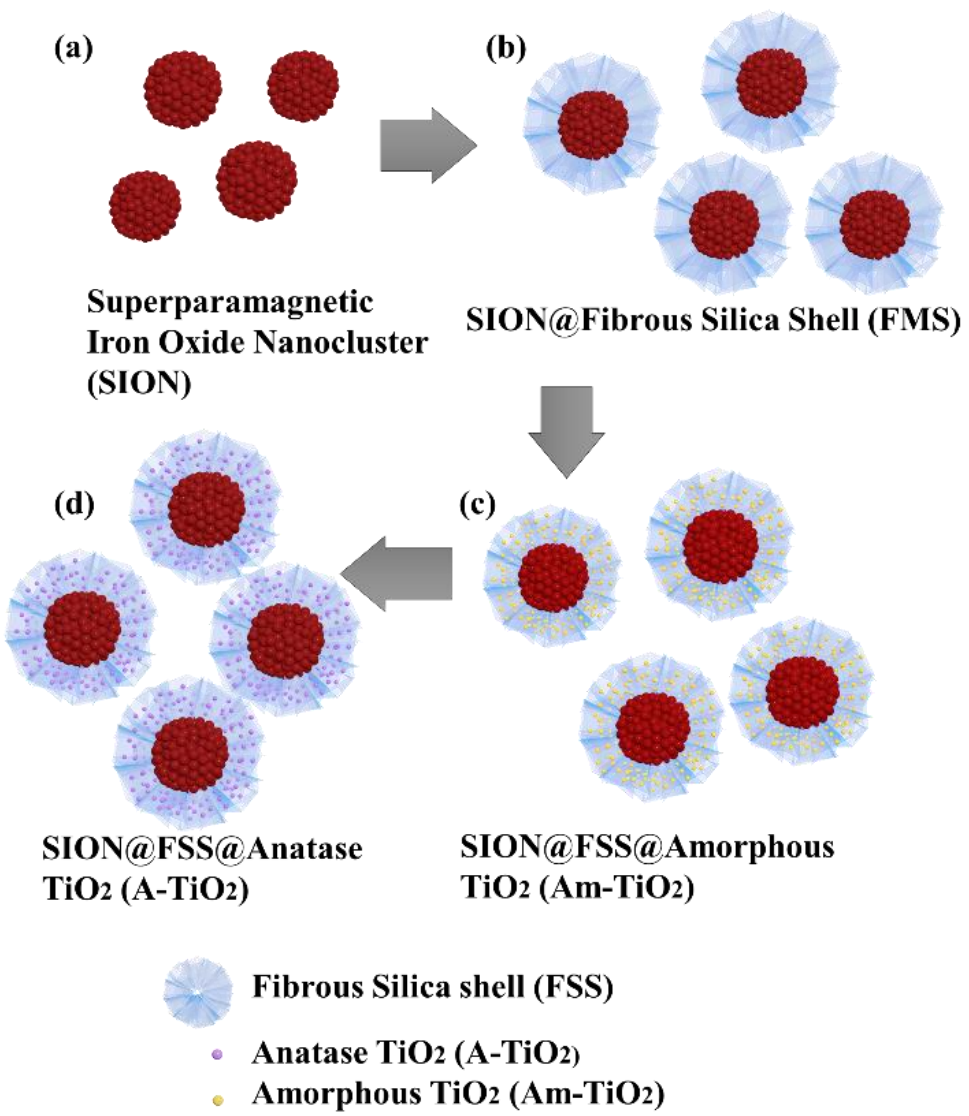

Figure 4 Schematic of the procedure for preparing magnetically recoverable photocatalyst: (a) SION, (b) SION@FSS, (c) SION@FSS@Am-TiO_2 and (d) SION@FSS@A-TiO_2.

The procedure for the synthesis of SION@FSS@A-TiO_2 involves three steps (**Figure 4**). First, the SIONs are homogeneously coated with dendritic FSS by a sol-gel process [31]. Next, amorphous TiO_2 nanoparticles were deposited on the FSS to form SION@FSS@Am -TiO_2, which undergo a hydrothermal reaction to yield the SION@FSS@A- TiO_2.

3.1.2. SION core

The starting SION has a raspberry-like shape, which is a conglobulation of 5–10-nm iron oxide nanocrystals packed into a 280 ± 37-nm nanoclusters (**Figure 5**) [51]. These SIONs combine the advantages of individual grains and confer an enhanced magnetic property [42].

3.1.3. FSS coating on SION core (SION@FSS)

The oil−water biphase stratification approach [31] was used to prepare a silica coating shell with fibrous large pores that enable enhanced adsorption and release ability. To generate such silica coating shells, SIONs were first dispersed in water and mixed with CTAB and TEA. Then, TEOS and 1-octadecene were added to the mixture; the mixture was hydrolyzed and condensed to generate the first FSS layer on SION. The second-layer generation step starts with discarding the oil layer and adding TEOS and decalin. The final layer is generated using a mixture of TEOS and cyclohexane as an oil-based solvent.

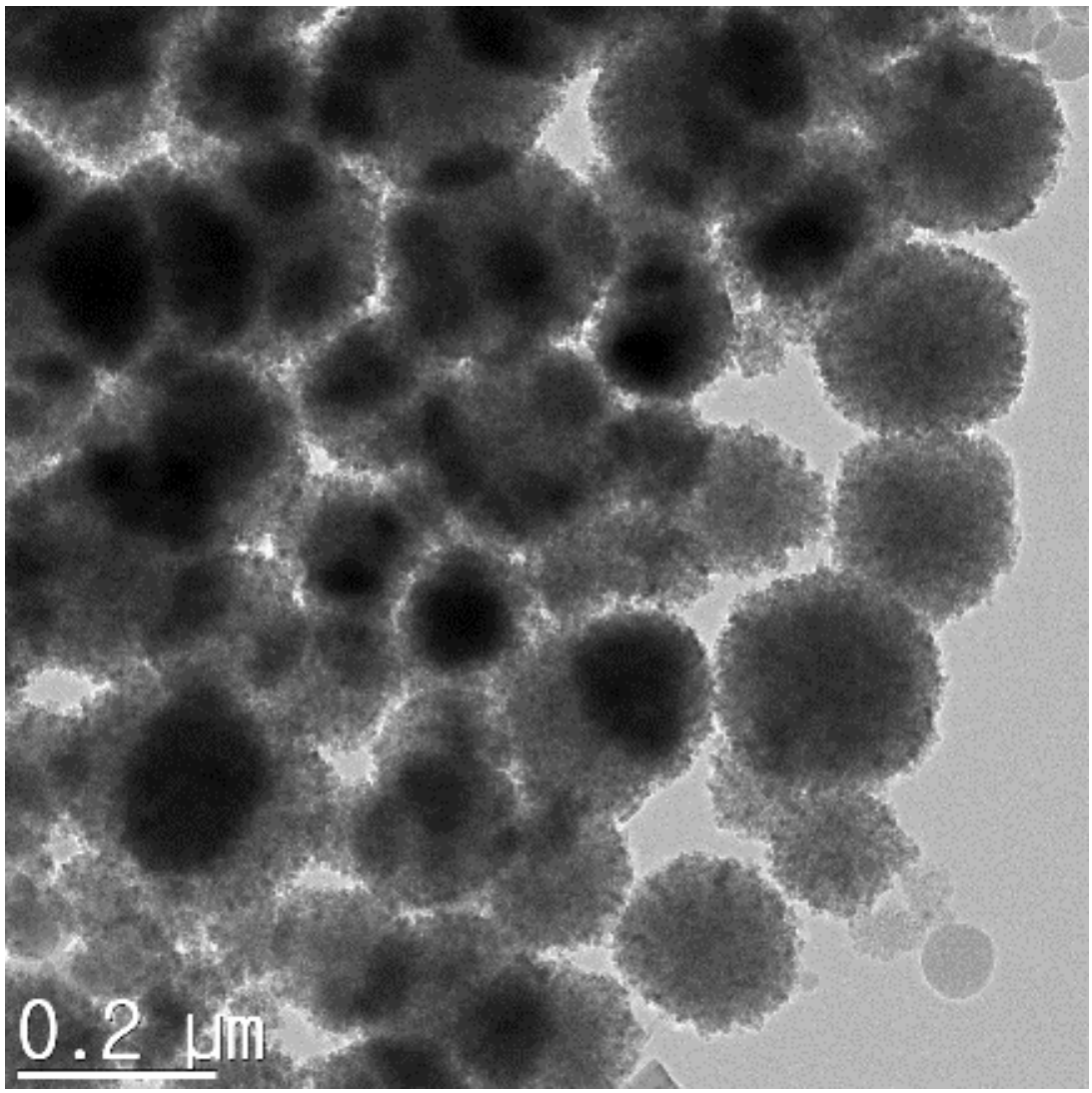

Figure 5. TEM image of the as-prepared superparamagnetic iron oxide nanocluster.

3.1.4. Control of FSS thickness

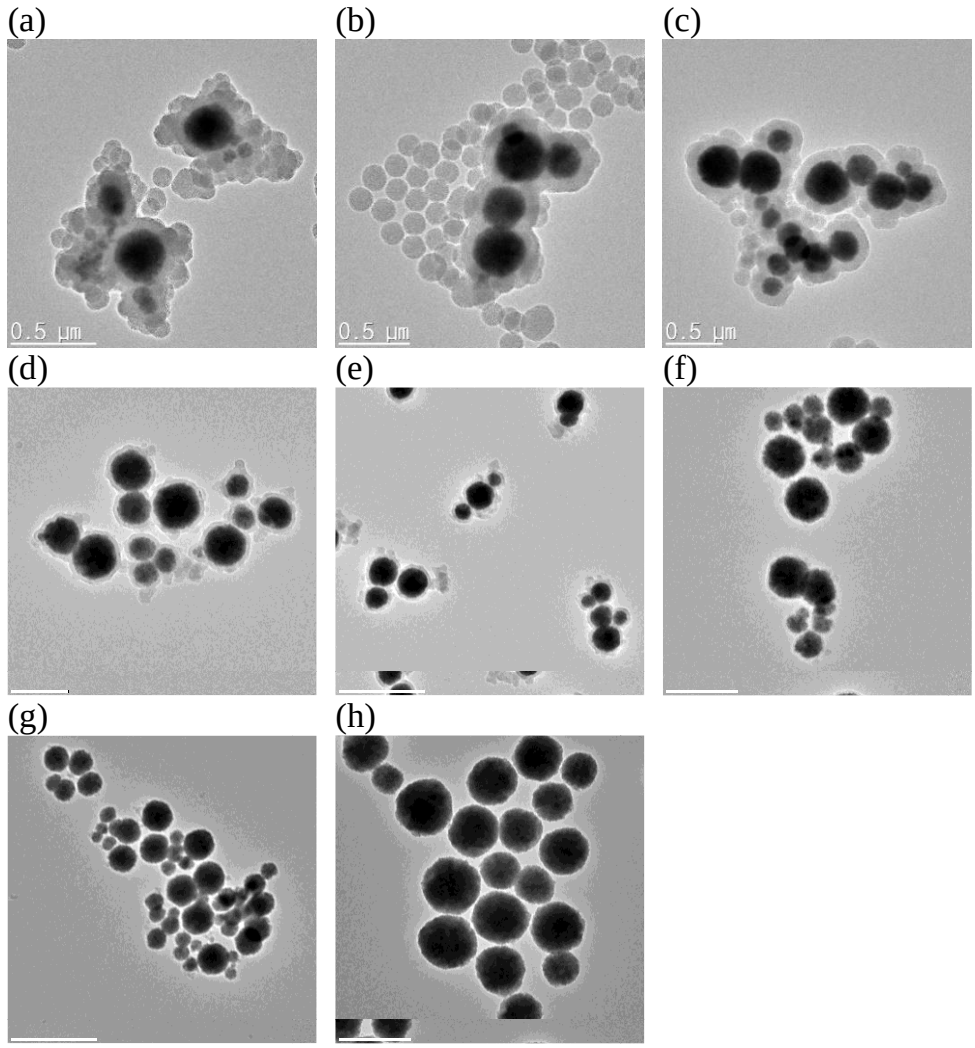

Figure 6. TEM images of the superparamagnetic iron oxide nanocluster core@fibrous silica shell nanocomposites after the first layer stratification synthesized with varying amounts of TEOS (a) 4 ml, (b) 1 ml, (c) 500 µl, ((d),(e)) 250 µl, ((f), (g)) 50 µl and (h) 12.5 µl for 6 h

For SION@FSS synthesis without residual FSS particles, the amount of TEOS was adjusted from 4 ml to 12.5 µl during the first layer stratification (**Figure 6**). When 4 ml of TEOS was added, SION@FSS spheres were fused with several FSS particles (**Figure 6** (a)). The aggregated FSS spheres were separated when the TEOS amount was reduced to 1 ml (**Figure 6** (b)), but SION@FSS agglomerates were still present. Separation of fused SION@FSS was obtained by gradually reducing the TEOS volume to 250 µl (**Figure 6** (b)-(e)). Fully separated SION@FSS nanoparticles started to appear on using 60 µl of TEOS (**Figure 6** (f)). By reducing the TEOS volume below 60 µl, the FSS layer becomes thinner and cannot be observed by TEM (**Figure 6** (g)-(h)).

3.1.5. Supporting TiO_2 on SION@FSS and crystallization

After removing residual CTABs by calcination, TBOT was added dropwise to an ethanolic solution of SION@FSS and water. Amorphous TiO_2 nanoparticles supported on SION@FSS were crystallized using the hydrothermal method.

EDX analysis (**Figure 9**) shows that iron and oxide spectra are dominant in the center of the particles and silica and titanium spectra dominate on the outer side of the particles.

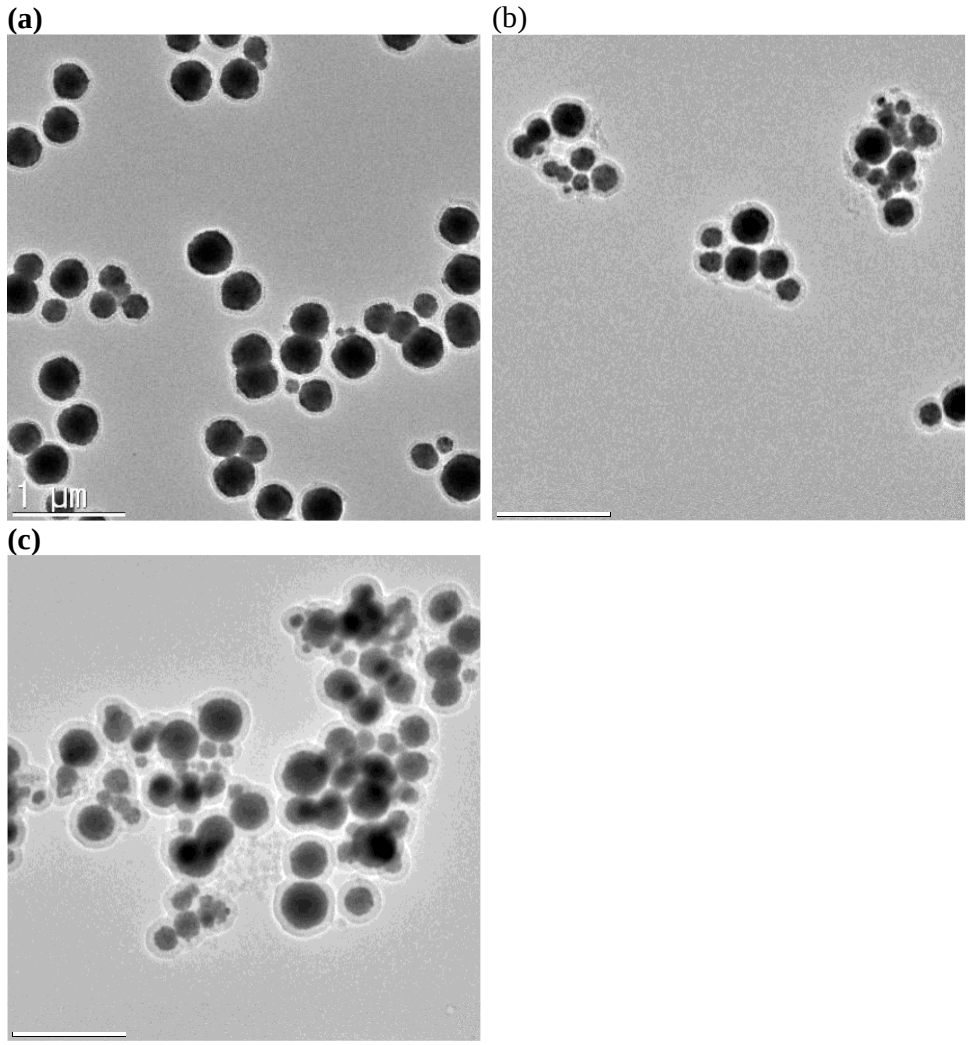

Figure 7 TEM images of the superparamagnetic iron oxide nanocluster core@fibrous silica shell nanocomposite at the end of the third stratification synthesized with varying amounts of TEOS (a) 50 µl, (b) 100 µl and (c) 200 µl.

3.1.6. Control of TiO_2 amounts

Likewise, silica layers were coated on single SION@FSS nanoparticles during the second and third layer generation steps (**Figure 7**) by controlling the TEOS volume.

To take advantage of their wide surface area and application in photocatalysis, TiO_2 spheres were confined in pores. To increase the filling amount without remnant TiO_2 spheres, the amount of TBOT was adjusted from 10 µl to 2 ml (**Figure 8**). Experimental results showed that 400–800 µl of TBOT was sufficient to fill in the FSS pores (**Figure 8** (b), (c)). When the TBOT concentration reached 1% (v/v), fused SION@FSS@Am-TiO_2 nanoparticles were observed (**Figure 8** (d)). Otherwise, when TBOT concentration was too low, considerable number of the FSS pores remained empty (**Figure 8** (a)). As a result, SION@FSS@Am-TiO_2 synthesized with 800 µl of the titanium precursor was used for further analysis.

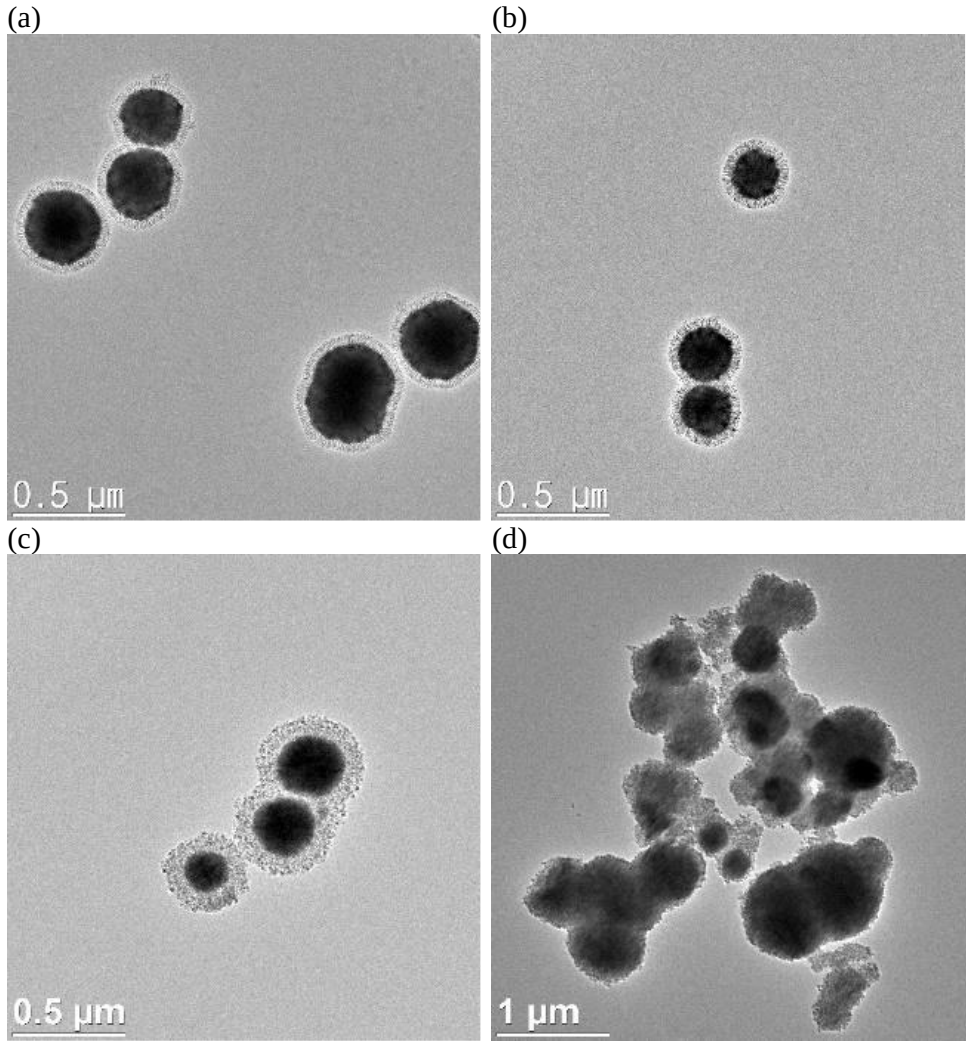

Figure 8 TEM images of SION@FSS@A-TiO_2 synthesized with varying amounts of TBOT (a) 10 µl, (b) 50 µl, (c) 800 µl and (f) 2 ml.

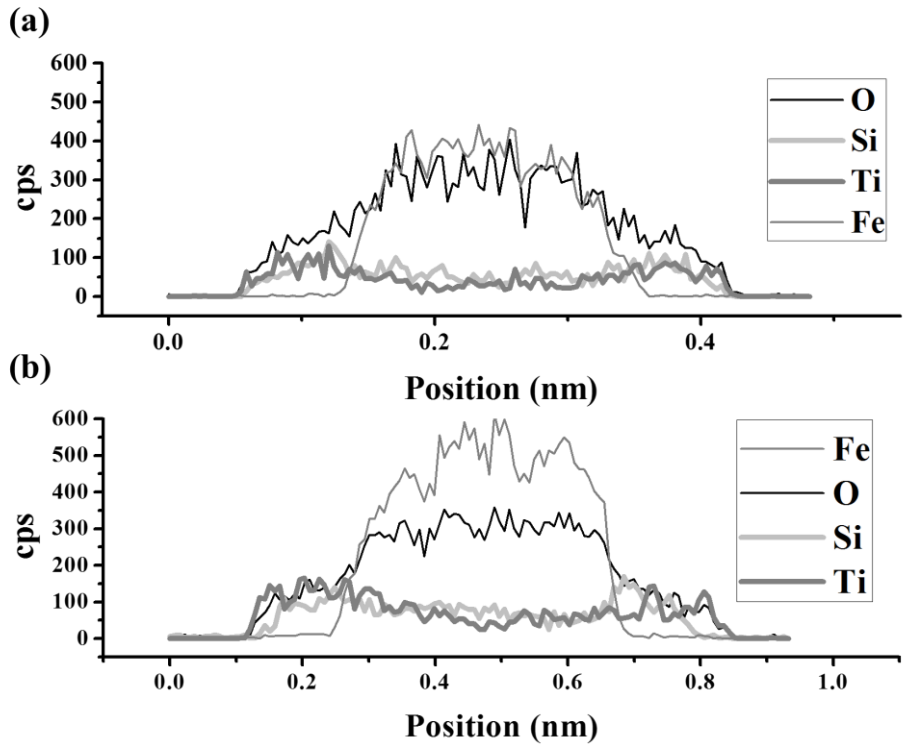

Figure 9 Energy-dispersive X-ray spectroscopy (EDS) spectrum of (a) SION@FSS@Am-TiO_2 and (b) SION@FSS@A-TiO_2.

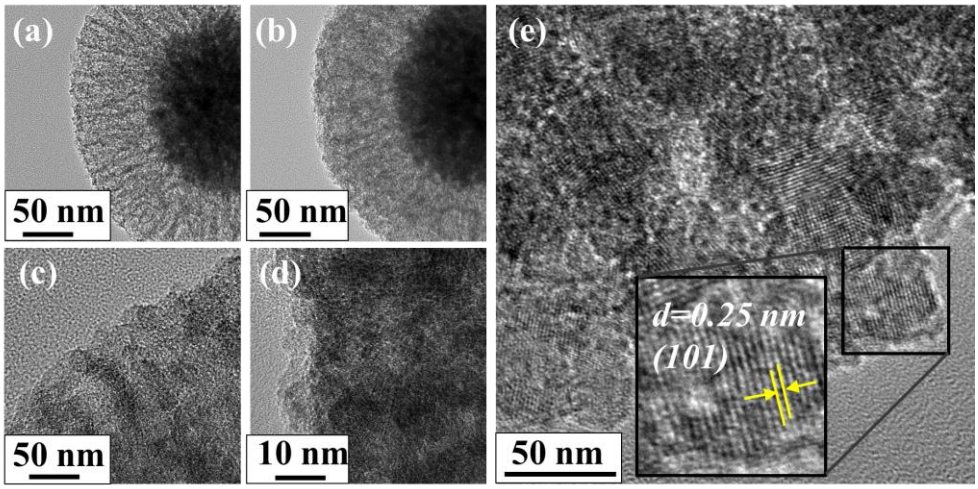

Figure 10. TEM images of IO@FSS@Am-TiO_2 showing Amorphous (a-d) to anatase phase transition of grafted titanium oxide nanoparticles. Lattice fringes correspond to (101) plane of anatase are found on IO@FSS@Am-TiO_2 (e). Amount of the TiO_2 precursor (TBOT) were adjusted to 400 µl ((a), (c) (magnified view)) and 800 µl ((b), (d) (magnified view)).

Titanium dioxide nanoparticle loading were verified from both TEM images (**Figure 10**) and EDX analysis (**Figure 9**). When 400 µl of TBOT was used (a), more pore voids between the FSS layers were observed compared to when 800 µl of TBOT was used (b). On magnified view, x30000, more TiO_2 nanoparticles were observed when 800 µl of TBOT was used (c) compared with that when 400 µl of TBOT (d). It shows high possibility of greater TiO_2 nanoparticles loading on SION@FSS@Am-TiO_2 by increasing the amount of titanium precursor. Loading of TiO_2 nanoparticles after hydrothermal reaction was determined by the crystalline structure the grains observed between the FSS layers, which matches the (101) plane of the anatase nanocrystals (e).

3.2. **characterization**

3.2.1. Size and morphology

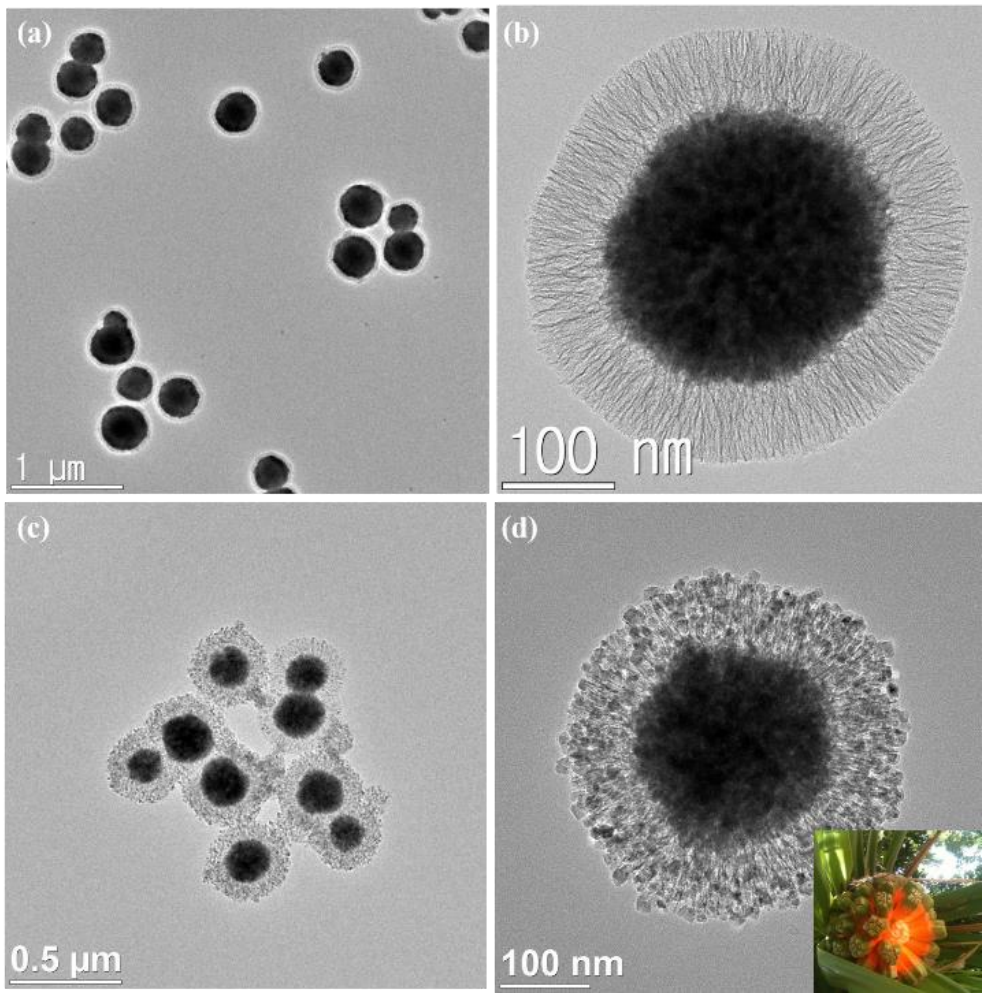

Figure 11. TEM images of SION@FSS (50 µl TEOS) at the end of the third layer growth (a, b) and SION@FSS@A-TiO_2 as a final product for water purification (c, d). Inset of (d) shows the picture of a screwpine which has a shape similar to that of SION@FSS@A-TiO_2.

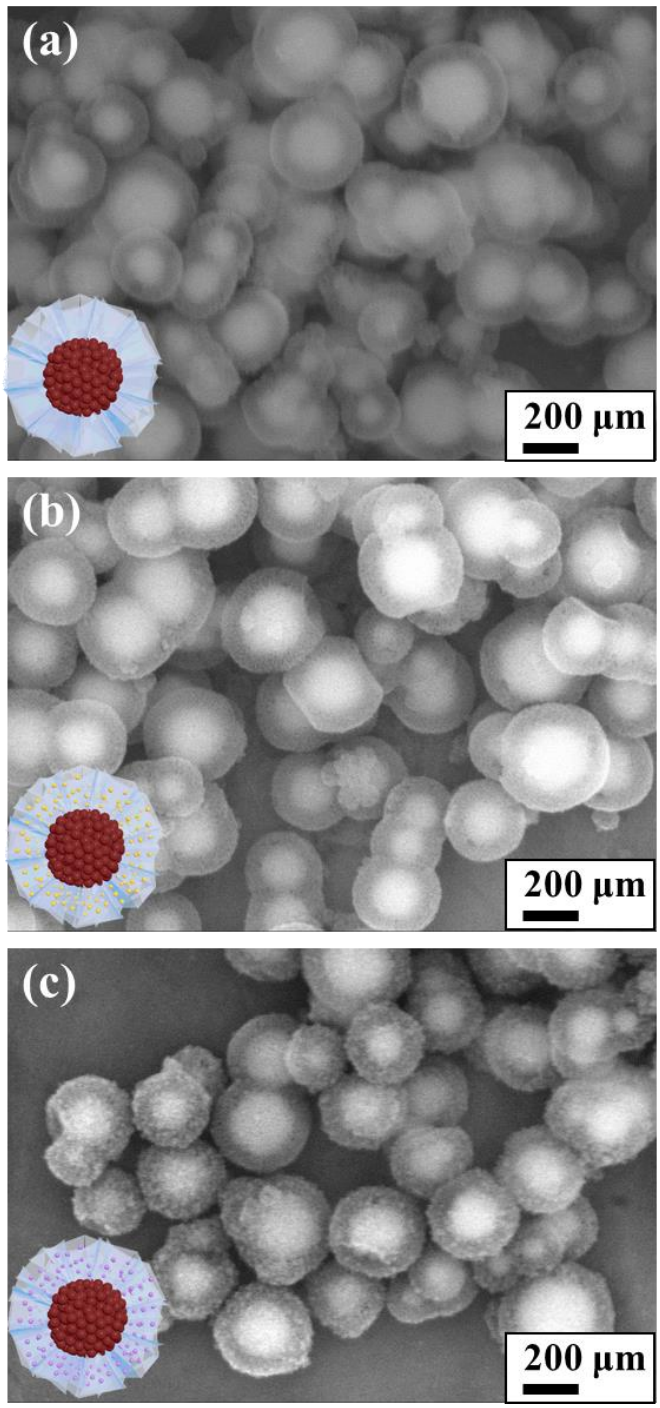

Figure 12. SEM images of (a) SION@FSS, (b) SION@FSS@Am-TiO_2 and (c) SION@FSS@A-TiO_2.

Fibrous silica shell with uniform layer thickness could be clearly seen in both TEM (**Figure 11**) and SEM images (**Figure 12**). Average size of SION@FSS was 317.7 ± 56.2 nm, as shown in the SEM images. The average layer thickness of SION@FSS was 71.1 ± 7.5 nm. SION@FSS shows wide size distribution owing to the polydispersity of the iron oxide cores, but the thickness of FSS is uniform irrespective of the size of the core. The size of prehydrothermal SION@FSS@Am-TiO_2 was 324 ± 50.0 nm and that of posthydrothermal SION@FSS@A-TiO_2 was 305 ± 37.9 nm, as derived from the SEM observations. The thickness of the coating FSS + Am-TiO_2 layer was 70.5 ± 9.1 nm. To crystalize the TiO_2 nanoparticle from amorphous to anatase phase, hydrothermal method is used due to low energy required compared to high temperature furnace method. After the posthydrothermal treatment, the layer shrunk a little to 68.9 ± 8.3 nm. It has been reported that silica could be partially etched during the hydrothermal treatment [33].

3.2.2. Crystal structure

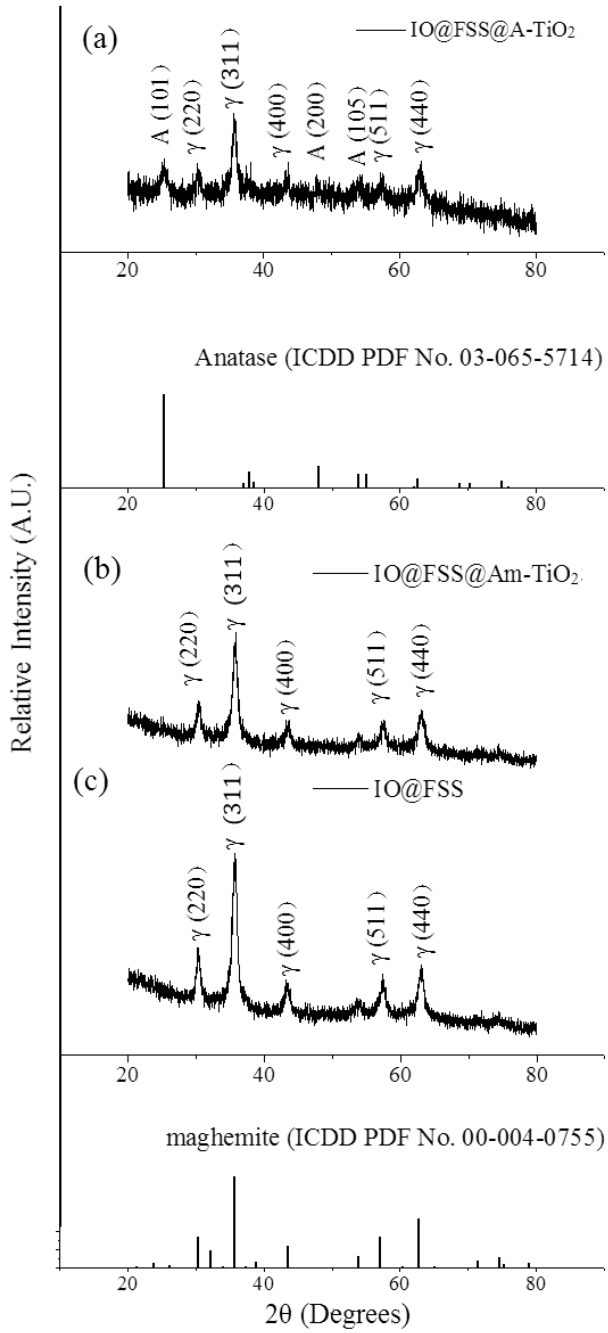

Figure 13. X-ray diffraction analysis of (a) SION@FSS@A - TiO_2 , (b) SION@FSS@Am-TiO_2 and (c) SION@FSS. Crystal planes are indexed with γ (maghemite) and A (anatase).

Since amorphous TiO_2 shows less photocatalytic activity compared to anatase TiO_2, the nanocomposite undergoes crystallization. The phases of the titanium-coated samples before and after the crystallization step were characterized by powder X-ray diffraction (XRD) (Figure 13). Prehydrothermal TiO_2 nanoparticles were amorphous as no SION@FSS@Am-TiO_2 spectrum (b) matched that of anatase (ICDD PDF card 03-06505714). Maghemite peaks or patterns are dominant in both XRD (Figure 13) and SAED (**Figure 14**) results, suggesting that the iron oxide core is maghemite in nature with polycrystalline structure. The core is initially magnetite [51], but undergoes transition to maghemite during the hydrothermal reaction.

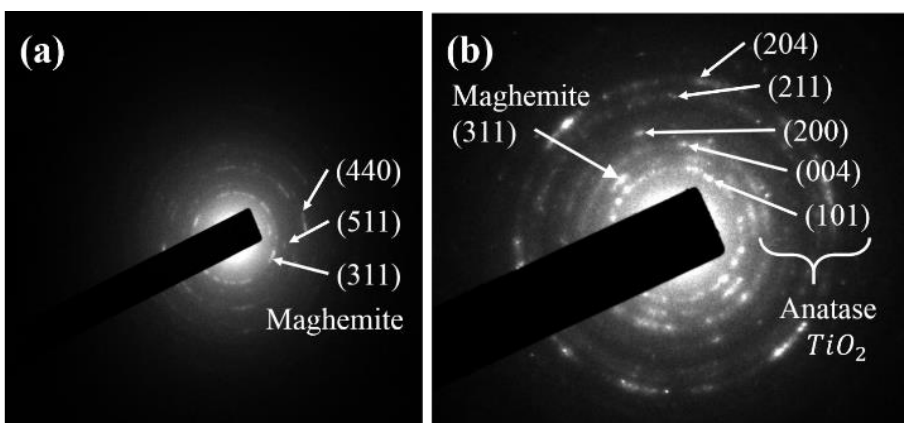

Figure 14. SAED patterns of (a) SION@FSS@Am-TiO_2 and (b) SION@FSS@A-TiO_2.

After the hydrothermal reaction, the diffraction spectrum obtained from SION@FSS@A-TiO_2 (**Figure 13** (a)) shows a peak at 25.3 ° corresponding to the (101) reflection of anatase. Peaks at 48.04 ° and 53.88 ° are attributed to the (200) and (105) planes, respectively, of the anatase-phase TiO_2 (ICDD PDF card 03-06505714). Although maghemite spectra are dominant in XRD, SAED analysis

clearly revealed the existence of other anatase planes. The five ring patterns in (Figure 14 (b)) correspond to the (204), (211), (200), (004), and (101) planes of anatase TiO_2. The most intense peak of SION@FSS@A-TiO_2 in the SAED patterns also corresponds to the (311) plane of maghemite. To sum up, appearance of anatase peaks prove the transition of amorphous to anatase phase of the supported TiO_2 after the hydrothermal treatment.

3.2.3. Pore structure analysis

Table 2 Morphological and textural characteristics of the nanoparticles

Sample Name	S_{BET} (m^2/g)	V_t (cm^3/g)	D_{BJH} (nm)
SION@FSS	265.62	0.745	11.22
SION@FSS@Am-TiO_2	237.07	0.434	8.39
SION@FSS@A-TiO_2	149.98	0.434	12.77

S_{BET}, Brunauer-Emmett-Teller pore surface area (m^2/g); V_t, Single-point adsorption total pore volume at P/P_o=0.994; D_{BJH}, Barrett-Joyner-Halenda adsorption average pore diameter.

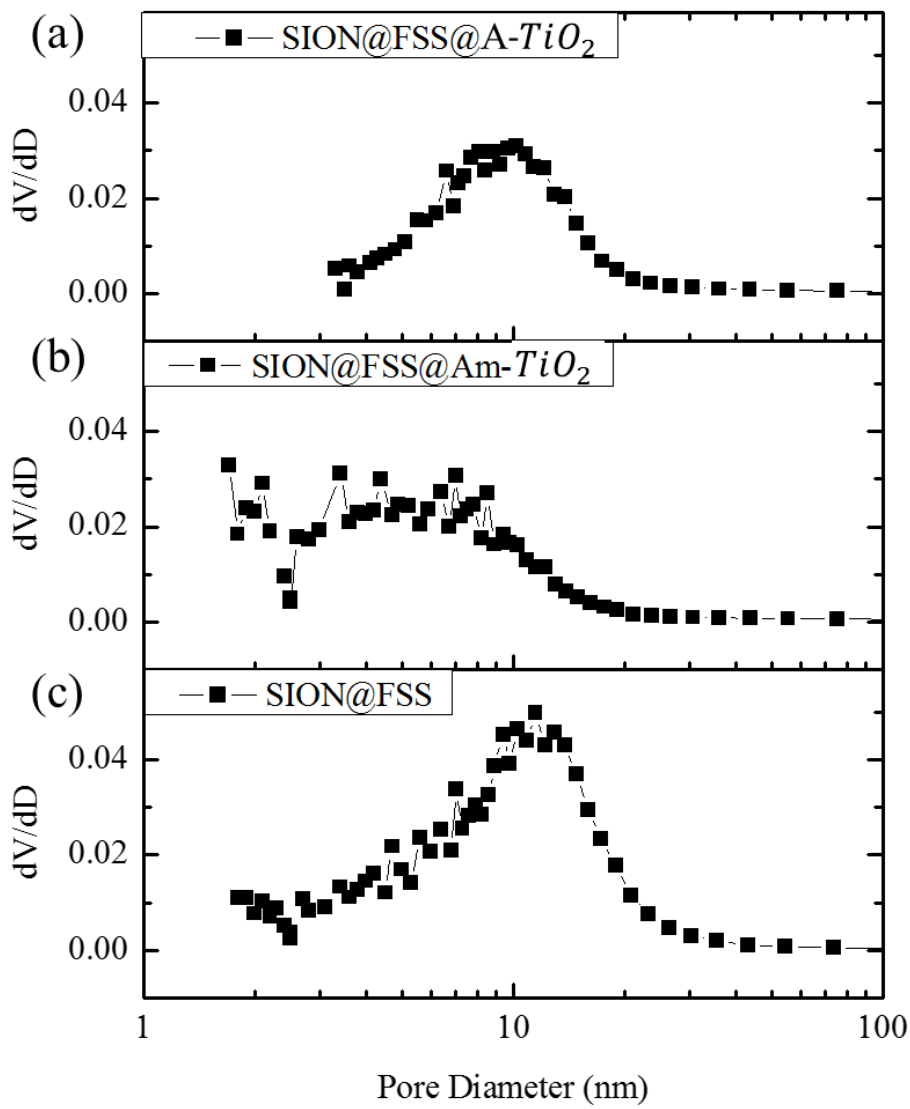

Figure 15 Pore size distributions of SION@FSS (a), SION@FSS@Am-TiO_2 (b) and SION@FSS@A-TiO_2 (c).

Morphological change at each synthesis step is summarized in the Table 1. Total pore volume of the SION@FSS spheres, 0.745 cm^3/g, match that of the FSS spheres from the previous report, 0.689 cm^3/g. Reduced surface area of SION@FSS@Am-TiO_2 confirms that TiO_2 is supported in the SION@FSS pores. During the hydrothermal reaction, amorphous TiO_2 undergoes crystallization and crystal growth, leading to the increased TiO_2 nanoparticle size. Thus, pores below 10 nm are absent from the pore size distribution graph of SION@FSS@Am-TiO_2 (**Figure 15**). Therefore, increased pore size after hydrothermal reaction is expected to be due to the removal of micropores and mesopores from between the TiO_2 nanoparticles [53]. This also leads to close packing of the TiO_2 nanoparticles, which reduces the SION@FSS@A-TiO_2 surface area to 149.98 m^2/g.

3.2.4. Magnetic property

The nanoparticles were recollected using the magnetic property of the iron oxide core. The graph of induced magnetization versus field shows saturation magnetization at 4.114 emu/g (**Figure 16**). Saturation magnetization of SION@FSS@Am-TiO_2 is low compared to that of the iron oxide core, owing to the presence of silica and TiO_2 that do not contribute to the magnetic induction. All the nanoparticles that were synthesized based on SION@FSS were dragged by a small handheld magnet and were redispersed easily by shaking the vials after withdrawing the magnet.

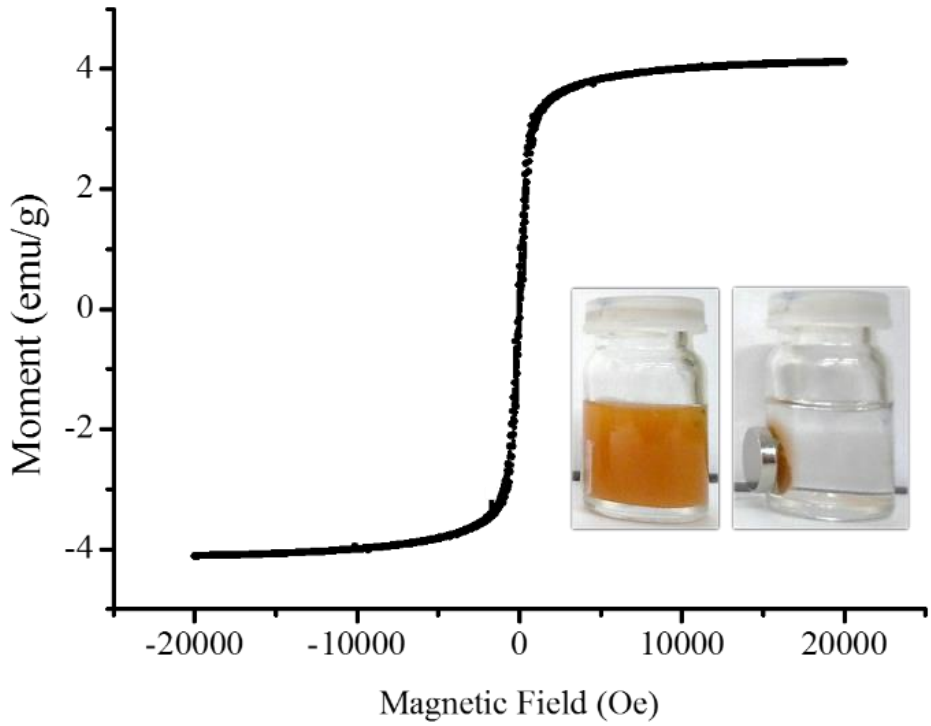

Figure 16 Field-dependence of magnetization graph of SION@FSS@A -TiO_2 measured at 20 K. Inset shows SION@FSS@A-TiO_2 dispersed in ethanol (left) and magnetically collected SION@FSS@A-TiO_2 (right).

3.3. **Photodegradation of MetB**

Finally, the catalytic effect of the anatase TiO_2 decorated on the particle surface is evaluated, after reaching the absorption-desorption equilibrium for 2hrs. MetB solution was purified using UV-illuminated catalyst nanoparticles, SION@FSS@A-TiO_2. With the aid of SION@FSS@A-TiO_2, 3 mg/L of dye molecules were degraded before 3 h of UV-irradiation (**Figure 17**).

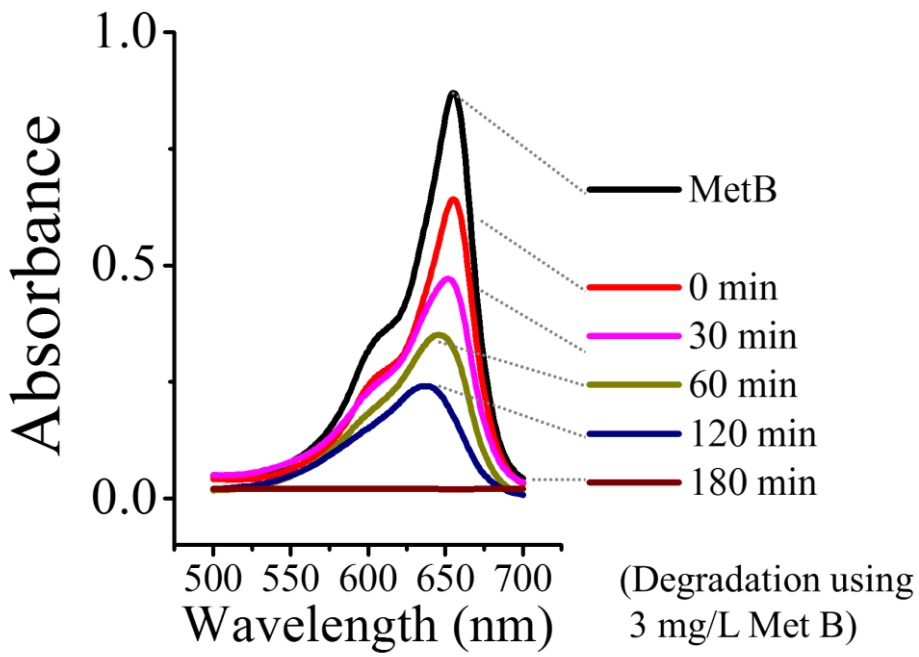

Figure 17 Uv-Vis absorbance spectra, which shows decreasing maximum absorbance after UV irradiation.

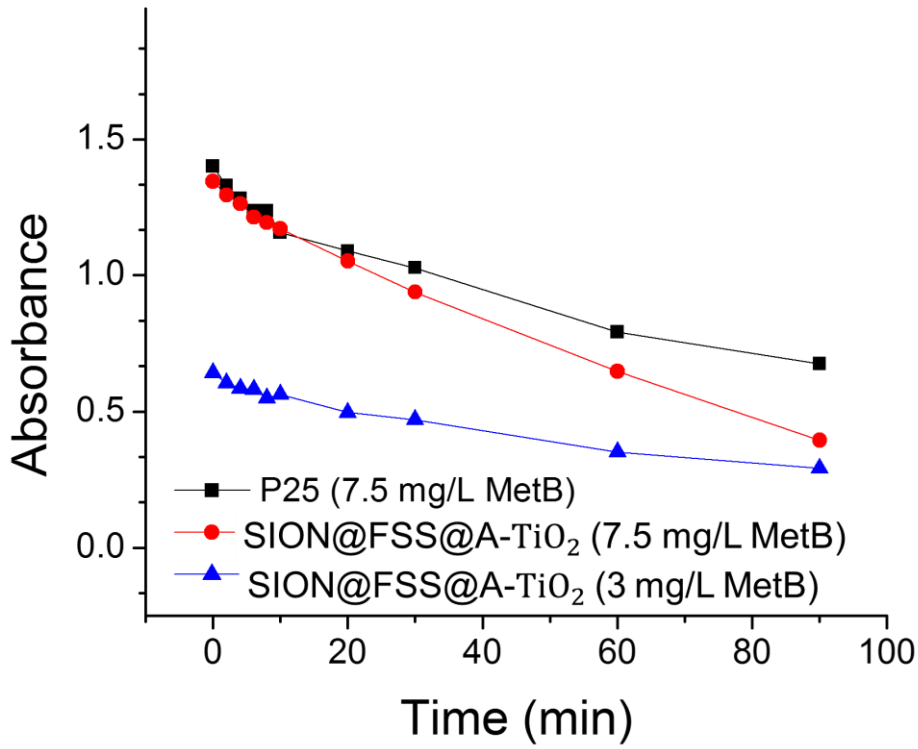

Figure 18 Degradation test of MetB solution with SION@FSS@A-TiO_2 and commertial P25.

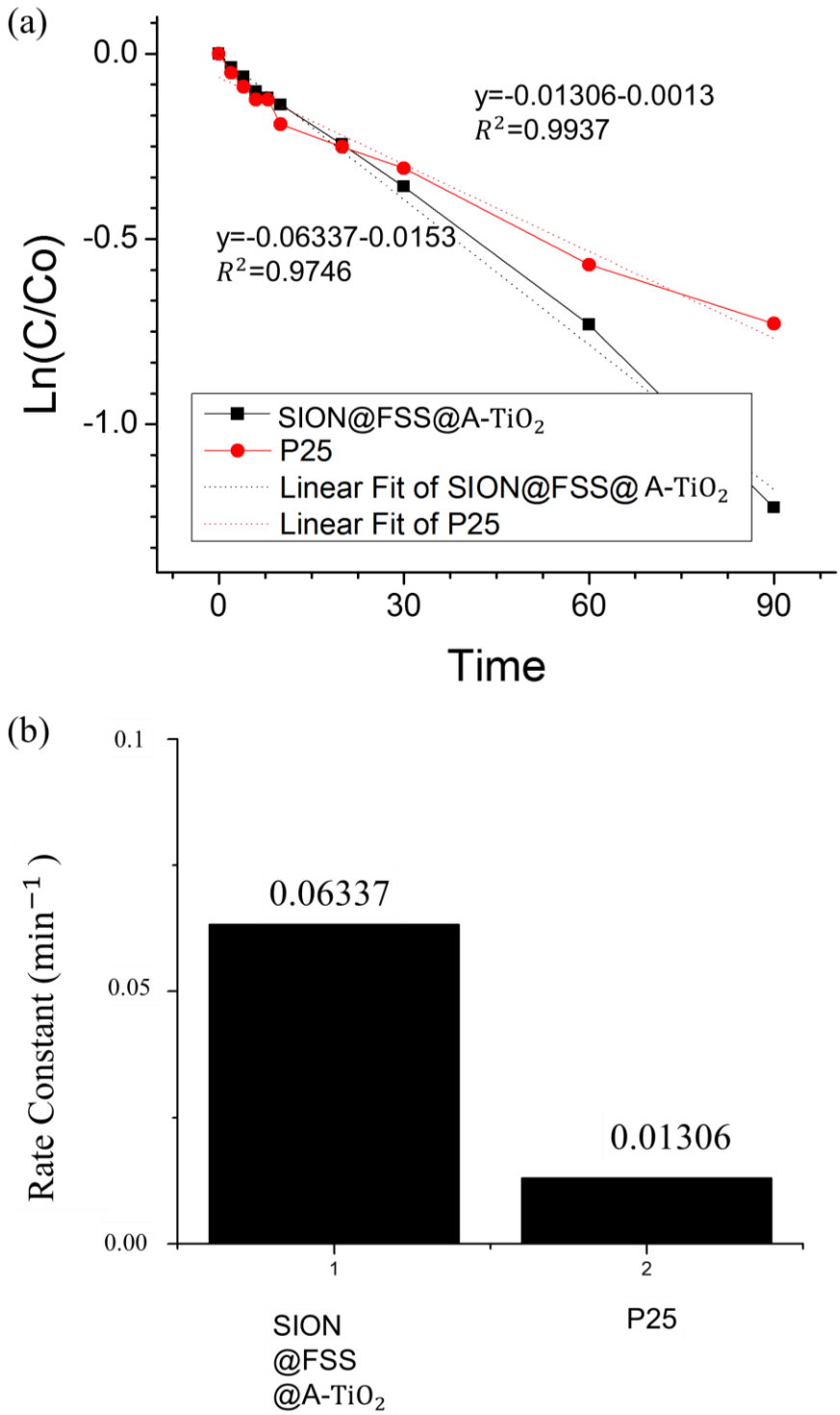

Figure 19 Rates of degradation evaluated (a) and compared with commercial P25 (b) using 7.5 mg/L MetB solution.

SION@FSS@A-TiO_2 shows much higher dye decomposition rate than same amount of commercial P25 TiO_2 nanoparticles (**Figure 18**, **Figure 19**). Since a considerable amount of non-catalytic materials are included in the mass of SION@FSS@A-TiO_2, rate constant might be higher for the reaction with catalysts, SION@FSS@A-TiO_2. Considering the very low first-order rate constant of an atase TiO_2 nanoparticles [54] and thin film [55] made in a similar manner without magnetic core and silica supports, the synthesis and the use of SI ON@FSS@A- TiO_2 may enhance the photocatalytic effect.

Finally, the nanoparticles were reused after the degradation (**Figure 20**). The recycled SION@FSS@A-TiO_2 shows less catalyst deterioration after the repeated trials while retaining its structure (**Figure 21**) at the end of the degradation trials.

The removal time and concentration of degraded MetB dye is compared with other magnetically recollectable nanocomposites with TiO_2 nanoparticles (**Table 3**). From the results, SION@FSS@A-TiO_2 show comparable degradation performance while considering the lamp intensity and amount of catalysts used

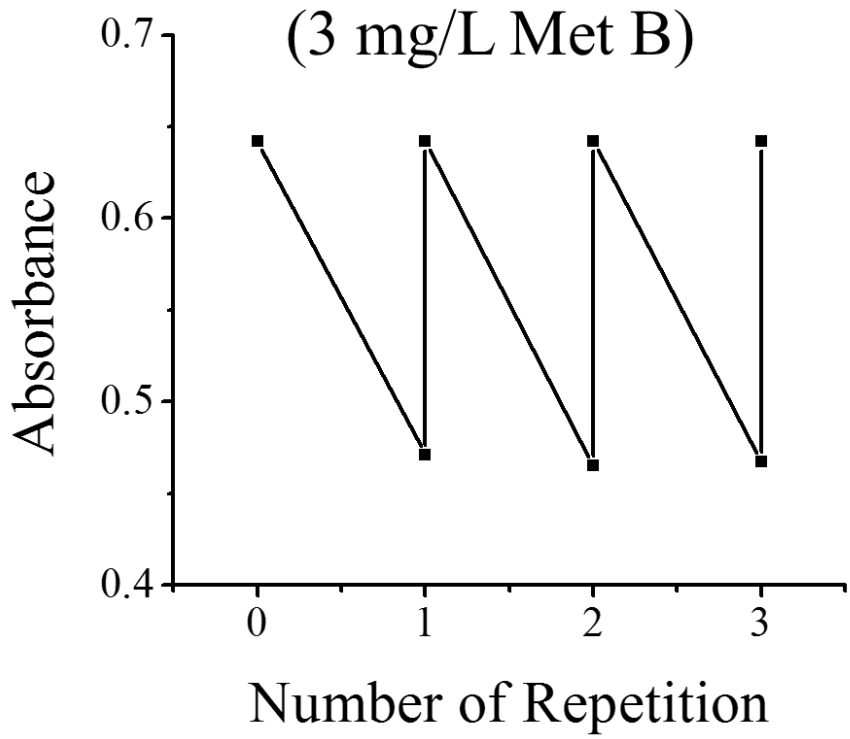

Figure 20 Repeated trials of dye degradation test performed using recovered SION@FSS@A-TiO_2 nanoparticles.

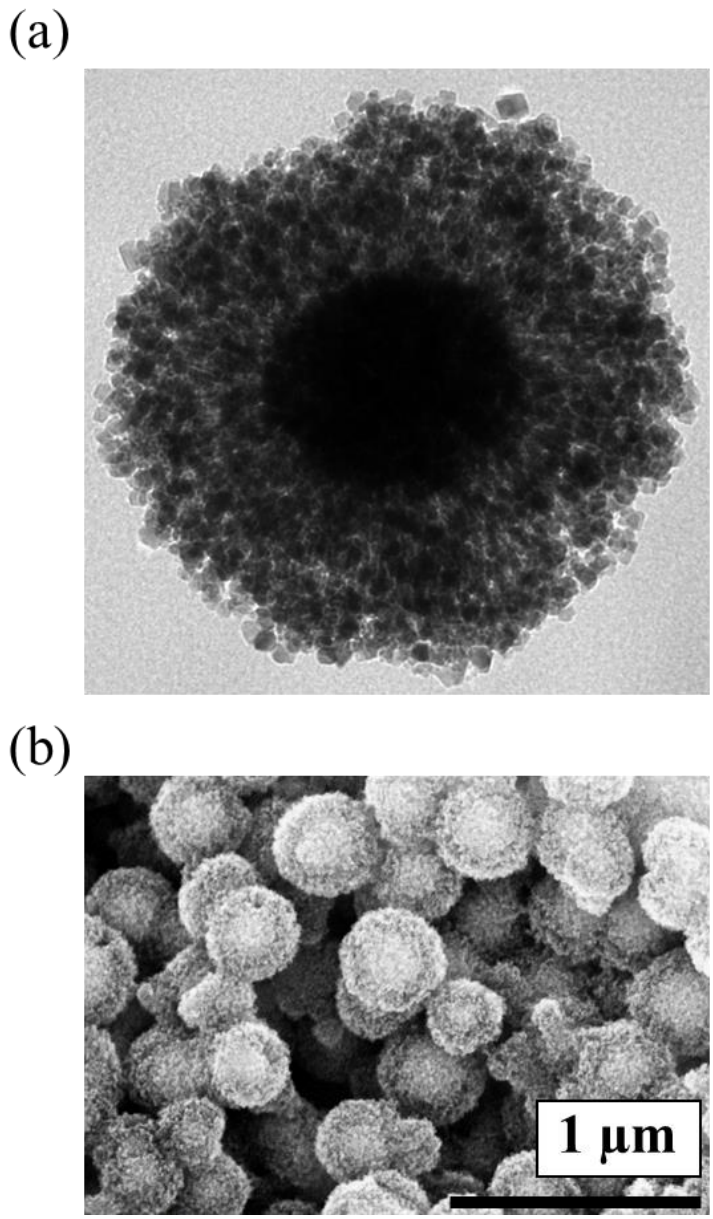

Figure 21 Retention of the morphology of SION@FSS@A-TiO_2 after repetitive dye degradation cycles.

Table 3 Comparison of MetB dye degradation using magnetically recollectable nanocomposites with TiO_2 nanoparticles.

Catalyst	Catalyst Concentration [mg/mL]	Time required for reaching adsorption-desorption equilibrium [hour]	MetB Concentration [mg/L]	Time required for complete dye removal [hour]	UV lamp Power [mW/cm^2 ,W]	UV wave length [nm]	Ref
Rattle Type Fe_3O_4 /SiO_2 /TiO_2	0.1	-	1	0.167	800,-	254	[30]
Fe_3O_4 @rGO @TiO_2	1.5	0.5	10	2	-,300	UV lamp with filter	[47]
SION @FSS @A-TiO_2	0.1	2	3	3	50, 48	312	This Work

Chapter 4. Conclusion

In summary, a magnetically recoverable photocatalyst was prepared by supporting TiO_2 nanoparticles on a superparamagnetic iron oxide nanocluster core@fibrous silica shell nanocomposite. Using the raspberry-shaped magnetic core as a seed, seed-mediated growth was used to form a fibrous silica shell (FSS), which enabled enhanced adsorption and release ability, directly on the iron oxide nanocluster surface. The FSS shell coating was repeated thrice to increase the pore radius of the core@shell nanostructures. FSS with fibrous-shaped large pores enables large amounts of nanoparticles to be easily supported on the pore surface.

The core@shell nanostructure was optimized to have a single core for each nanoparticle by adjusting the amount of the silica source. Amorphous TiO_2 supported on a superparamagnetic iron oxide nanocluster core@fibrous silica shell nanocomposite was crystallized to the anatase phase (SION@FSS@A-TiO_2), as it shows a good photocatalytic effect. When used for water purification, the screwpine-shaped SION@FSS@A-TiO_2 shows higher dye degradation kinetics compared to commercial P25 nanoparticles. Additionally, the presence of a magnetically inducible SION core in SION@FSS@A-TiO_2 enables its recollection from water after use.

References

[1] D. Paraschiv, C. Tudor and R. petrariu, *Sustainability*, 2015, **7**, 1280-1291.

[2] H. Hettige, M. Mani and D. Wheeler, *J. Dev. Econ.*, 2000, **62**, 445-476.

[3] C. A. Gonzales, E. Riboli and G. Lopez-Abente, *Am. J. Ind. Med.*, 1988, **14**, 673-680.

[4] J. S. Bae and H. S. Freeman, *Dyes Pigm.*, 2007, **73**, 81-85.

[5] O. J. Hao, H. Kim and P. C. Chiang, *Critical Reviews in Environmental Science and Technology*, 2000, 30, 449-505.

[6] X. Li and Y. Zhao, *Water Sci. Technol.*, 1997, **36**, 165-172.

[7] J. Augustynski, *Electrochim. Acta*, 1993, **38**, 43-46.

[8] V. H. Grassian, A. Adamcakova-Dodd, J. M. Pettibone, P. I. O'shaughnessy and P. S. Thorne, *Nanotoxicology*, 2007, **1**, 211-226.

[9] C. M. Sayes, R. Wahi, P. A. Kurian, Y. Liu, J. L. West, K. D. Ausman, D. B. Warheit and V. L. Colvin, *Toxicol. Sci.*, 2006, **92**, 174-185.

[10] J. G. Ayres, P. Borm, F. R. Cassee, V. Castranova, K. Donaldson, A. Ghio, R. M. Harrison, R. Hider, F. Kelly and I. M. Kooter, *Inhal. Toxicol.*, 2008, **20**, 75-99.

[11] T. Kuhlbusch, H. Krug and K. Nau, *Annexe F: Article*, 2009.

[12] J. A. Byrne, B. R. Eggins, N. M. D. Brown, B. McKinney and M. Rouse, *Appl. Catal., B.*, 1998, **17**, 25-36.

[13] A. Fernández, G. Lassaletta, V. M. Jiménez, A. Justo, A. R. González-Elipe, J. M. Herrmann, H. Tahiri and Y. Ait-Ichou, *Appl. Catal., B.*, 1995, **7**, 49-63.

[14] D. Zhao, J. Feng, Q. Huo, N. Melosh, G. H. Fredrickson, B. F. Chmelka and G. D. Stucky, *Science*, 1998, **279**, 548-552.

[15] C. Kresge, M. Leonowicz, W. Roth, J. Vartuli and J. Beck, *nature*, 1992, **359**, 710-712.

[16] Z. Luan, E. M. Maes, P. A. W. van der Heide, D. Zhao, R. S. Czernuszewicz and L. Kevan, *Chem. Mater.*, 1999, **11**, 3680-3686.

[17] Y. Xu and C. H. Langford, *J. Phys. Chem. B*, 1997, **101**, 3115-3121.

[18] B. J. Aronson, C. F. Blanford and A. Stein, *Chem. Mater.*, 1997, **9**, 2842-2851.

[19] R. Singh, R. Bapat, L. Qin, H. Feng and V. Polshettiwar, *ACS Catal.*, 2016, **6**, 2770-2784.

[20] R. van Grieken, J. Aguado, M. J. López-Muñoz and J. Marugán, *J. Photochem. Photobiol.*, 2002, **148**, 315-322.

[21] V. Polshettiwar, D. Cha, X. Zhang and J. M. Basset, *Angew. Chem. Int. Ed.*, 2010, **49**, 9652-9656.

[22] X. Huang, Z. Tao, J. C. Praskavich, A. Goswami, J. F. Al-Sharab, T. Minko, V. Polshettiwar and T. Asefa, *Langmuir*, 2014, **30**, 10886-10898.

[23] D.-S. Moon and J.-K. Lee, *Langmuir*, 2012, **28**, 12341-12347.

[24] X. Du and J. He, *Langmuir*, 2011, **27**, 2972-2979.

[25] X. Du and S. Z. Qiao, *Small*, 2015, **11**, 392-413.

[26] A. Fihri, D. Cha, M. Bouhrara, N. Almana and V. Polshettiwar, *ChemSusChem*, 2012, **5**, 85-89.

[27] Q. Qu, Y. Min, L. Zhang, Q. Xu and Y. Yin, *Anal. Chem.*, 2015, **87**, 9631-9638.

[28] X. Du, X. Li and J. He, *ACS Appl. Mater. Interfaces*, 2010, **2**, 2365-2372.

[29] K. Zhang, L.-L. Xu, J.-G. Jiang, N. Calin, K.-F. Lam, S.-J. Zhang, H.-H. Wu, G.-D. Wu, B. Albela, L. Bonneviot and P. Wu, *J. Am. Chem. Soc.*, 2013, **135**, 2427-2430.

[30] D.-S. Moon and J.-K. Lee, *Langmuir*, 2014, **30**, 15574-15580.

[31] D. Shen, J. Yang, X. Li, L. Zhou, R. Zhang, W. Li, L. Chen, R. Wang, F. Zhang and D. Zhao, *Nano Lett.*, 2014, **14**, 923-932.

[32] J. Liu, S. Z. Qiao and Q. H. Hu, *Small*, 2011, **7**, 425-443.

[33] S. Linley, T. Leshuk and F. X. Gu, *ACS Appl. Mater. Interfaces*, 2013, **5**, 2540-2548.

[34] M. Ye, Q. Zhang, Y. Hu, J. Ge, Z. Lu, L. He, Z. Chen and Y. Yin, *Chem. Eur. J.*, 2010, **16**, 6243-6250.

[35] S. Kurinobu, K. Tsurusaki, Y. Natui, M. Kimata and M. Hasegawa, J. *Magn. Magn. Mater*, 2007, **310**, e1025-e1027.

[36] L. Zhao, Y. Chi, Q. Yuan, N. Li, W. Yan and X. Li, *J. Colloid Interface Sci.*, 2013, **390**, 70-77.

[37] S. Watson, D. Beydoun and R. Amal, *J. Photochem. Photobiol.*, 2002, **148**, 303-313.

[38] F. Chen, Y. Xie, J. Zhao and G. Lu, *Chemosphere*, 2001, **44**, 1159-1168.

[39] F. Chen and J. Zhao, *Catal. Lett.*, 1999, **58**, 246-247.

[40] A. H. Lu, E. E. Salabas and F. Schüth, *Angew. Chem. Int. Ed.*, 2007, **46**, 1222-1244.

[41] J. Ge, Y. Hu, M. Biasini, W. P. Beyermann and Y. Yin, *Angew. Chem. Int. Ed.*, 2007, **46**, 4342-4345.

[42] O. Gerber, B. P. Pichon, C. Ulhaq, J.-M. Grenèche, C. Lefevre, I. Florea, O. Ersen, D. Begin, S. Lemonnier, E. Barraud and S. Begin-Colin, *J. Phys. Chem. C*, 2015, **119**, 24665-24673.

[43] Z. Sun, H. Li, D. Guo, J. Sun, G. Cui, Y. Liu, Y. Tian and S. Yan, *J. Mater. Chem. C*, 2015, **3**, 4713-4722.

[44] J. Yang, D. Shen, Y. Wei, W. Li, F. Zhang, B. Kong, S. Zhang, W. Teng, J. Fan, W. Zhang, S. Dou and D. Zhao, *Nano Res.*, 2015, **8**, 2504-2514.

[45] K. Yu, X. Zhang, H. Tong, X. Yan and S. Liu, *Mater. Lett.*, 2013, **106**, 151-154.

[46] T. Atabaev, J. H. Lee, J. J. Lee, D. W. Han, Y. H. Hwang, H. K. Kim and N.

H. Hong, *Nanotechnology*, 2013, **24**, 345603.

[47] M. Tadic, S. Kralj, M. Jagodic, D. Hanzel and D. Makovec, *Appl. Surf. Sci.*, 2014, **322**, 255-264.

[48] L. Kopanja, S. Kralj, D. Zunic, B. Loncar and M. Tadic, *Ceram. Int.*, 2016, **42**, 10976-10984.

[49] L. Kopanja, I. Milosevic, M. Panjan, V. Damnjanovic and D. Makovec, *Appl. Surf. Sci.*, 2016, **362**, 380-386.

[50] M. Tadic, I. Milosevic, S. Kralj, M. Mbodji and L. Motte, *J. Phys. Chem.* C, 2015, **24**, 13868-13875.

[51] J. Liu, Z. Sun, Y. Deng, Y. Zou, C. Li, X. Guo, L. Xiong, Y. Gao, F. Li and D. Zhao, *Angew. Chem. Int. Ed.*, 2009, **121**, 5989-5993.

[52] J. Lee, M. Othman, Y. Eom, T. Lee, W. Kim and J. Kim, *Micropor. Mesopor. Mat.*, 2008, **116**, 561-568.

[53] J. Yu, G. Wang, B. Cheng and M. Zhou, *Appl. Catal., B.*, 2007, **69**, 171-180.

[54] S. Senthilkumaar, K. Porkodi and R. Vidyalakshmi, *J. Photochem. Photobiol. A Chem.*, 2005, **31**, 225-232.

[55] N. R. Mathews, E. R. Morales, M. A. Cortés-Jacome and J. T. Antonio, *Solar Enery*, 2009, **83**, 1499-1508.

요약(국문초록)

초상자성 산화철 나노클러스터 중심@방사형 실리카 피막의 나노복합체에 이산화티타늄 나노입자가 부착된 재사용이 가능한 광촉매에 대한연구

본 연구에서는 초상자성을 지닌 산화철 나노클러스터 (SION) 중심@방사형 실리카 셸 구조 (FSS) 위에 TiO_2나노입자를 담지하여 재사용가능한 나노구조 복합체(SION@FSS@Am-TiO_2)를 합성하였다. 작은 산화철 입자들이 모여 큰 산화철을 이루는 라즈베리 모양의 산화철을 중심으로 하여 균일한 두께의 FSS껍질을 솔-겔 방법으로 코팅하였다. 이 때 실리카 전구체의 양을 조절하여 각 나노입자복합체당 하나의 라즈베리 모양의 산화철 입자만을 갖도록 하였다. FSS껍질은 방사형으로 기공이 펼쳐진 구조를 가져 많은양의 TiO_2를 기공표면에 담지할 수 있는 장점이 있다. 이 SION@FSS (중심@껍질) 구조 지지체 위에 무정형의 TiO_2를 담지한 후 (SION@FSS@Am-TiO_2), TiO_2의 광촉매효과를 향상하기 위해 수열합성을 통해 아나타제로 결정화 하였다(SION@FSS@A-TiO_2). 합성된 나노구조 복합체는 광촉매 효과를 보였으며 상용 P25와 비교하여 빠른 염료분해속도를 보였다. 또한, 본 나노구조 복합체는 염료분해 이후 자성을 이용하여 재수거 및

재사용이 가능하도록 설계되었다.

주요어 : 방사형 실리카 나노입자, 광촉매, 코어 쉘, 염료분해, 재사용 가능 나노입자

학 번 : 2014-24838